

The Rotor-Stator Study of E-Core Hybrid Flux Switching Motor

J. Abd Rani, E. Sulaiman, M.Z Ahmad and F. Amin

Faculty of Electrical and Electronic Engineering, Universiti Tun Hussein Onn Malaysia, Parit Raja,
Batu Pahat, 86400 Johor, Malaysia.
he150066@siswa.uthm.edu.my

Abstract—This paper explores the combination of stator and rotor of a hybrid flux switching motor (HFSM) through a rotor-stator study on E-core stator type of HFSM. The plausible combination of rotor and stator are analysed through open circuit condition to verify the principles of HFSM on the proposed structures and closed-circuit condition to examine the capabilities of the verified structures. The structure producing the highest torque is undergone structural optimisation to refine the performance.

Index Terms—HFSM; E-Core Hybrid Flux Switching Motor; Rotor-Stator Study; Finite Element Analysis.

I. INTRODUCTION

The electrical energy utilisation globally was estimated between 60% to 70% of the energy production [1], [2]. The influence of new technology is affecting all branches of engineering including the electrical motor. The global demand for reducing greenhouse emission gas changed the trends of internal combustion engine on vehicles by employing alternative technology such as electrical motor on vehicles.

The shift of technology influences the introduction of the new technology of electrical motor such as flux switching motor to substitute the conventional electric motor such that induction motor, DC motor, and synchronous motor.

Although the concept of flux switching motor (FSM) was founded in the 1950s, the motor was marginalised in applications for decades [3]. The discovery of FSM deduces the advantage of the motor having great criteria for electric vehicle application. The structure of the rotor is a single part of the iron core without the presence of the permanent magnet and winding coil. The absence of a permanent magnet and winding coil on the stator make the rotor structure very robust without the need for thermal management to the rotor part [4]. Therefore, the flux generated by the winding coil or permanent magnet located mainly on the stator can be fully utilised for flux control hence making FSM very favourable motor for high-speed application such as an electric vehicle.

In the past decades, FSM had attracted the attention of many academicians to explore further the capability of FSM by dynamically varying the structure without compromising the principle of FSM [4]. The exploration of FSM gave birth to the concept of field excitation flux switching motor (FEFSM) and permanent magnet flux switching motor (PMFSM)[5]. The idea of FEFSM is the source of the flux is solely funded by the field excitation coil flux with the armature coil subsidise the connection between the magnetic circuit and the electrical circuit of the motor. While the PMFSM flux is originated from the permanent magnet

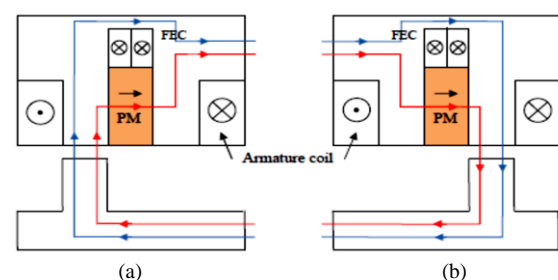
located in the motor.

The concept of field excitation coil and permanent magnet funding the motor was then combined hence the introduction of hybrid flux switching motor (HFSM) [6]. The fundamental characteristics of HFSM are flux regulation capabilities, avoidance of demagnetisation effects, extensive speed range and high torque-speed capability.

This paper aims to seek a structure of HFSM which substantially produce high torque and high-power motor with considerably great efficiency. In section I, the operating principle of HFSM is first introduced. The methodology, electrical parameters and geometrical parameters of HFSM are defined in section III. Then, in section III the rotor-stator study is conducted and verified by 2D finite element analysis (FEA) to deduce the plausible combination of numbers of rotor and stator for HFSM. The structure having the highest torque is optimise to refine the performance of the motor in section IV. Finally, section V will conclude the findings of this paper.

II. OPERATING PRINCIPLE

The operating principle of the HFSM is illustrated in Figure 1. The red line indicates the permanent magnet flux and the red line indicate field excitation flux. The term hybrid came from the fluxes due to field excitation coil and permanent magnet coil [7]. The combined forces of the flux creating a strong magnetic field, which influences the rotation of the rotor. In Figure 1(a) and Figure 1(b), the permanent magnet flux and field excitation flux are in the same polarity creating strong magnetic force leading to flux strengthening. Also, Figure 1(c) and Figure 1(d) illustrated the field excitation flux are both in the reverse polarity to permanent magnet polarity making the motor in flux weakening state.



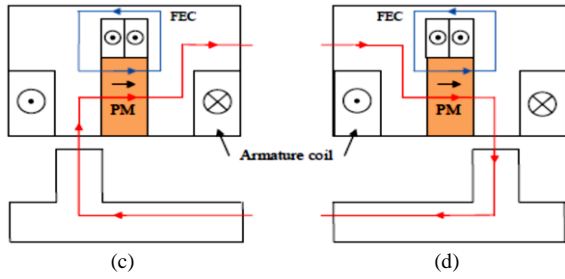


Figure 1: Operating Principle of HFSM

III. METHODOLOGY

The rotor-stator study of HFSM started off with the identification of rotor poles combinations with the number of stator poles. Figure 2 shows the structure of HFSM with E-Core stator partaking in the rotor-stator study. The combination number of stator slot and rotor poles were identified using Equation (1) [8]. Table 1 shows the combination of rotor poles and stator poles available for HFSM according to Equation (1).

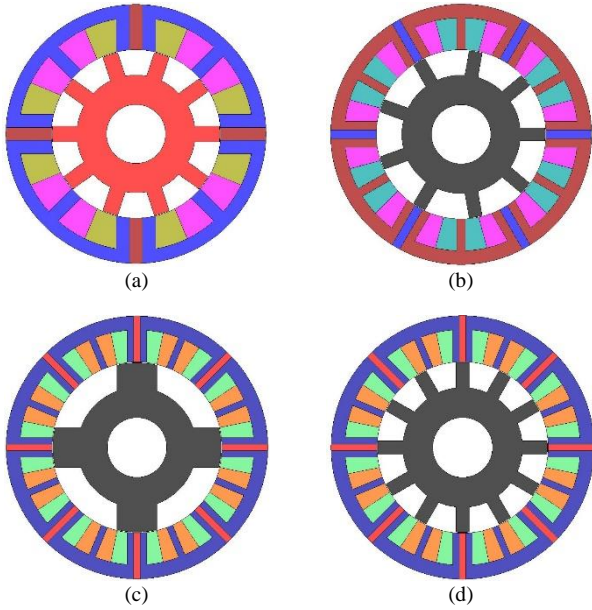


Figure 2: Design of HFSM for stator-rotor study (a) 4S10P (b) 6S9P (c) 8S4P (d) 8S12P

 Table 1
Rotor-Stator Combination

		Rotor Poles, N_r				
Stator	4	2	6	8	10	12
Slot, N_s	6	3	9	12	15	18
	8	4	12	16	20	24

$$N_r = N_s \left[1 \pm \frac{k}{2q} \right] \quad (1)$$

where: N_r = Rotor poles
 N_s = Stator slot
 k = Integer number
 q = Phase number

Table 2 demonstrated the fixed parameters that will be employed in the open circuit and closed-circuit condition of the 2D-FEA. HFSM is made up of two winding coils which

are field excitation coil and armature coil. The field excitation coil will be injected with 360 A_{rms} current, and the armature coil will be injected with 50 A DC current. During the closed circuit analysis, the armature current and field excitation current will be varied, and the maximum value on which both can be varied is set at 30 A_{rms}/mm² and 30 A/mm², respectively [9]. The relationship between the maximum armature current and armature density current as well as field excitation current and field excitation density current are demonstrated in Equation (2) and Equation (3), respectively.

 Table 2
Parameters Restriction

Fixed Parameters	HFSM
Maximum voltage (V)	650
Maximum armature current (A _{rms})	360
Maximum field excitation current (A)	50
Maximum armature current density, J_a (A _{rms} /mm ²)	30
Maximum field current density, J_e (A/mm ²)	30
Volume of PM (kg)	1.3
Outer stator diameter (mm)	264
Shaft diameter (mm)	60
Stack length (mm)	70
Air gap length (mm)	0.8

$$A_{rms} = \frac{J_A \alpha_A S_A}{N_A} \quad (2)$$

where

A_{rms} = Armature current
 J_A = Armature current density
 α_A = Filling factor
 S_A = Armature slot area
 N_A = Armature coil turn

$$A = \frac{J_E \alpha_E S_E}{N_E} \quad (3)$$

Where

A = Field excitation current
 J_E = Field excitation current density
 α_E = Filling factor
 S_E = Field excitation slot area
 N_E = Field excitation coil turn

Regarding geometrical parameters restriction cover the volume of the permanent magnet, outer stator diameter, shaft diameter, air gap length and stack length.

IV. ROTOR POLE ANALYSIS

A. Open Circuit Condition

The open circuit condition was conducted to confirm the coil arrangements and the direction of the permanent magnets in HFSM are operating the with FSM operating principle.

Figure 3 shows the flux generated by 4S10P HFSM, 6S9P HFSM, 8S4P HFSM and 8S12P HFSM due to the permanent magnet. The sinusoidal waveform of flux generated to confirm the operating principle of HFSM when no armature current and field excitation current injected into the motor.

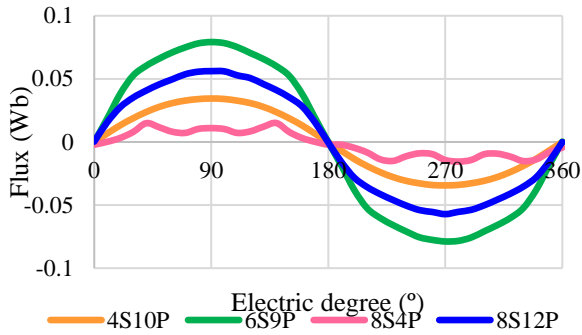


Figure 3: Flux due to permanent magnet at no load condition of 4S10P, 6S9P, 8S4P and 8S12P HFSM

With the operating principle, the four designs proceed to the next analysis, which is counter electromotive force analysis. Counter electromotive force analysis observes the magnetic condition of the motor when only field excitation current and the permanent magnet are a presence [10]. Figure 4 shows the variety of induced voltage occurred in all four designs when maximum field excitation current was applied.

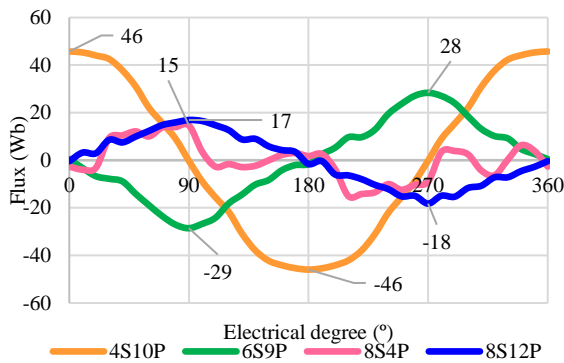


Figure 4: Counter electromotive force of 4S10P, 6S9P, 8S4P and 8S12P HFSM

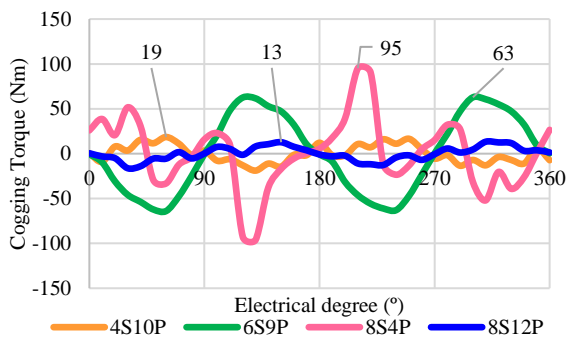


Figure 5: Cogging torque of 4S10P, 6S9P, 8S4P and 8S12P HFSM

The observation found that 4S10P exhibit the highest peak-to-peak counter electromotive force (CEMF) among all the designs at 46 Wb. Another observation that can be made is the value of peak-to-peak of the CEMF decrease with increasing number of stator slot. 6S9P HFSM registered peak-to-peak value at 28 Wb, 8S4P HFSM reduced to 17 Wb and lastly the 8S12P HFSM peak-to-peak CEMF is 14 Wb. High CEMF means the net voltage across the motor due to the relative motion of the armature coil and the magnetic fields belongs to permanent magnet and field excitation coil. Comparing the CEMF exhibited by all four topologies shows 4S10P had the least mini ripples compared to other

topologies. 8S4P registered the worst mini ripples on the flux linkage in one electric cycles.

Under the same condition of injected maximum field excitation current density and zero armature current, the cogging torque of 4S10P HFSM, 6S9P HFSM, 8S4P HFSM and 8S12P HFSM were observed. All topologies exhibit undesirable torque ripples and harmonics. The highest maximum cogging torque is 95 Nm from 8S4P topology, followed by 63 Nm of 6S9P HFSM, 19 Nm from 4S10P HFSM and 13 Nm from 8S12P HFSM. Further refinement needs to be conducted to mitigate the cogging torque, as a high percentage of cogging to the output torque is very unattractive. The poor effect of production torque amplified through vibration during the period the motor operates at low torque. The higher the cogging torque the vibration become more evident during low torque operating state. Several techniques identified in previous research (reference) capable of reducing the amplitude of cogging torque towards a favourable percentage of 10% of the output torque.

B. Closed Circuit Analysis

The performance of 4S10P HFSM, 6S9P HFSM, 8S4P HFSM and 8S12P HFSM were measured based on output torque at maximum field excitation current density. Figure 6 shows the output torque for the four topologies at maximum field excitation current with increasing injected armature current translated as armature current density.

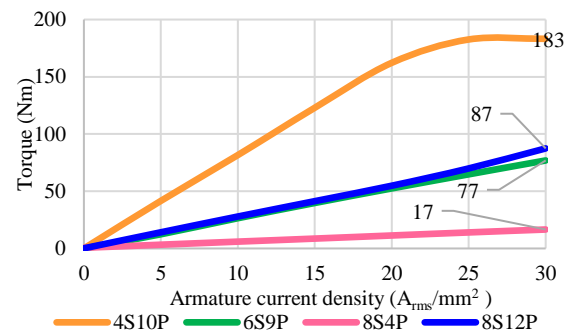


Figure 6: Output torque at maximum J_e of 4S10P, 6S9P, 8S4P and 8S12P HFSM

4S10P registered the highest torque performance at 183 Nm. Both 6S9P HFSM and 8S12P HFSM exhibit torque within close range to each other, which are 77 Nm and 87 Nm, respectively. Furthest down with the lowest output torque is 8S4P HFSM with 17 Nm.

Regarding output torque exhibited with increasing armature current density, 4S10P demonstrated a steep increase of torque production with increasing injected armature current. The steep increase reflects the fast response of the motor with increasing armature current. 6S9P HFSM and 8S12P HFSM have a steady increase of output torque but lean compared to 4S10P HFSM. Meanwhile, 8S4P HFSM has the smallest increase in torque from zero armature current until maximum armature current. This reflects 8S4P HFSM have the slowest pick-up than 6S9P HFSM and 8S4P HFSM. On the other note, both 6S9P HFSM and 8S4P HFSM have identical torque response and slower reaction compared to 4S10P HFSM.

V. OPTIMIZED DESIGN ANALYSIS

From section III and section IV, the open circuit condition and closed circuit condition had deduced the plausible topologies among all the designs for optimisation is 4S10P HFSM. The choice was made based on the open circuit and closed circuit profiling. 4S10P HFSM had perfectly flux linkage denoted by Figure 3. High CEMF and low cogging torque shown in Figure 4 and Figure 5, respectively strengthen the candidacy of 4S10P HFSM. Most importantly, 4S10P HFSM exhibited the highest and justifiable output torque that superseded the average output torque of the electric motor for electric vehicle application.

The topologies of 4S10P HFSM was refined with five cycles of optimisation by improving the design performance through parameter update. Figure 7 shows the optimised design of 4S10P HFSM with the topology and coil arrangement. Figure 7(b) indicated the armature coil arrangement with dark red colour. The armature coils were arranged coiling around the stator poles and a permanent magnet in one direction. Meanwhile, the field excitation coil indicated by yellow colour illustrate alternate polarity of winding in each set of coils.

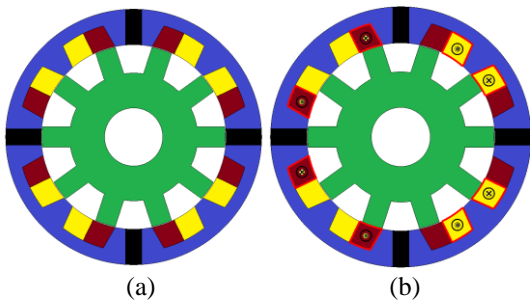


Figure 7: Optimized design of 4S10P HFSM (a) topology and (b) coil arrangement.

A. Flux Characteristics

The flux characteristics denoted by flux distribution and flux linkage is illustrated in Figure 8. Figure 8(a) shows the flux produced at maximum field excitation current density and maximum armature current density is uniformly distributed over the stator and the rotor. The white area on the stator side of Figure 8(a) indicated low flux is utilising the stator area while the red area indicated a high concentration of flux with the possibility of flux leakage. The leakage occurred due to the jumping medium for the flux to flow from stator to rotor.

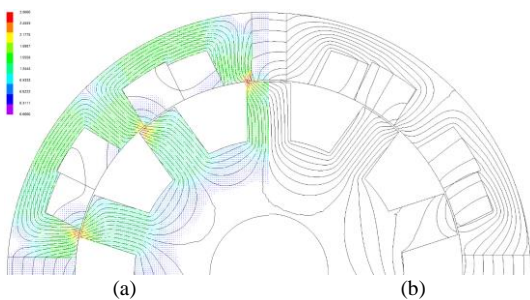


Figure 8: Flux characteristics of 4S-10P (a) Flux distribution (b) Flux linkage

B. CEMF

The CEMF of an optimised design of 4S10P HFSM was tested with maximum flown excitation current and zero armature current. The rotor freely rotated at a speed of 12 000 rpm due to the magnetic force caused by the interaction of field excitation coil and the permanent magnet. The maximum peak-to-peak value of CEMF is at 173 Wb illustrated in Figure 9. The waveform of the CEMF is not sinusoidal due to the third harmonic order of initial flux. The optimised design exhibited CEMF four times higher than the initial topology of 4S10P HFSM. The high magnitude of CEMF is favourable for regenerative braking system charging for the electric vehicle but unattractive attributes for cogging torque.

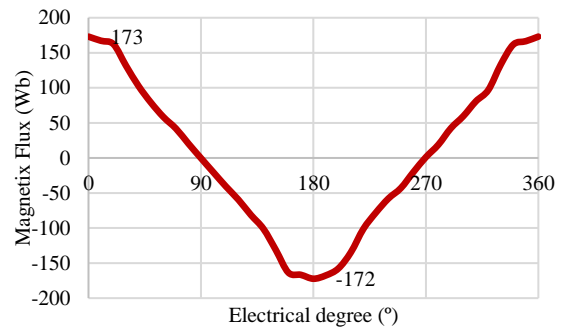


Figure 9: Induced voltage of 4S-10P

C. Cogging Torque

Figure 10 shows two cycles of cogging torque happened due to the interaction between the permanent magnet and laminated iron stator. The maximum cogging torque of optimised 4S10P HFSM increases five times from the initial topology at 173 Nm. Even with high cogging torque, the moment inertia of the rotor will diminish the cogging torque at high speed.

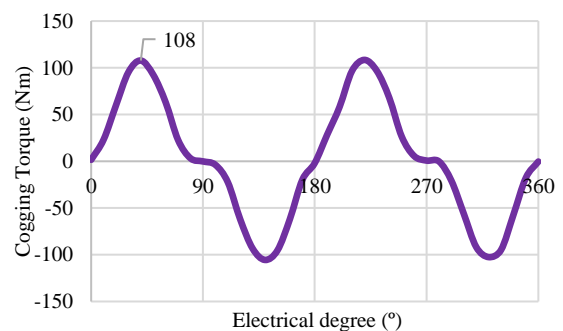


Figure 10: Cogging torque of 4S-10P

D. Torque-Speed Characteristic

The torque speed characteristic of 4S10P HFSM is defined in Figure 11. The blue line indicates the power of 4S10P HFSM. The power reaches the peak point of 72 kW with the corresponding speed of 4036 rpm. Meanwhile, the red line shows the torque characteristics of 4S10P HFSM with increasing speed. The torque peaking at 243 Nm as the speed accelerates from 0 rpm to 2863 rpm then the torque diminishes as the speed increase further. Correlatively with power output, the power achieves the peak value below the torque peak value at 203 Nm.

The high torque production at low speed can be inferred by the high production of flux. As the speed increase, the flux

production decreases hence reducing the torque production. At higher speed, the design experienced power loss due to iron loss and copper loss, which can be further minimised by increasing rotor pole arc angle and motor winding factor, respectively.

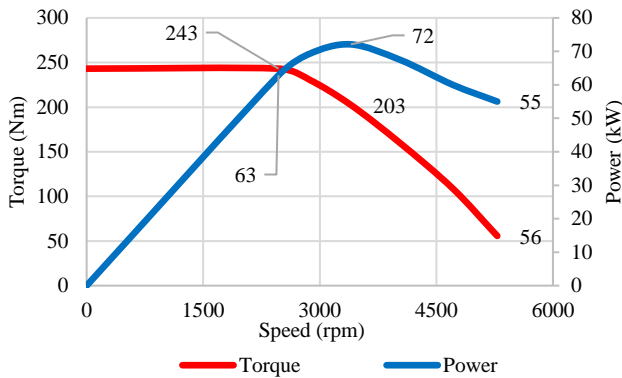


Figure 11: Torque-power vs speed characteristic of 4S10P

Table 3
Loss and efficiency of 4S-10P

No	P_{c-a} [kW]	P_{c-fec} [kW]	P_{i-s} [kW]	P_{i-rot} [kW]	P_{out} [kW]	Efficiency [%]
1	1.58	11	12.57	2.95	62.86	80.19
2	1.58	0.31	1.88	6.14	30.84	79.35
3	1.58	4.89	6.46	0.95	21.21	74.09
4	1.58	4.89	6.46	1.99	42.41	83.39
5	1.58	4.89	6.46	2.06	63.62	88.19
6	0.39	1.22	1.62	2.27	10.78	73.53
7	0.39	1.22	1.62	3.13	21.56	81.98
8	0.39	1.22	1.62	2.7	32.34	88.22

E. Loss and Efficiency.

The summary of iron loss, copper loss, and efficiency at eight operating points are concluded in Table 3. The efficiency reached 80.19% at operation point No. 1 with an output power of 62.86 kW. At operating point No. 2, the efficiency dropped to 79.35% with an output power of 30.84 kW. Operating point No. 1 and No. 2 are selected when the motor operates at maximum torque and maximum speed, respectively.

Operating point No. 3 to No. 8 denoted the loss prediction and motor efficiency covering operating range below 203 Nm. Within the operating range less than 203, the efficiency varied from 74.09 kW up to 88.22 kW. High copper losses contributed to the efficiency degradation rather than iron losses.

VI. CONCLUSION

The rotor-stator study was religiously enforced on 4S10P HFSM, 6S9P HFSM, 8S4P HFSM and 8S12P HFSM. Four topologies were first tested under open circuit condition and closed-circuit condition to confirm the operating principles and initial performance. Based on the initial performance, 4S10P HFSM exhibited the highest output torque was chosen to be further optimised to refine the performance. The optimisation managed to increase the output torque from 183 Nm up to 243 Nm along. At maximum torque, the motor recorded 80.19% efficiency. High efficiency, high torque with flux regulation capabilities from varying the field excitation current are desirable positive attributes for various application such as electric vehicles.

ACKNOWLEDGEMENT

This work was supported by Incentive Grant Scheme for Publication, IGSP (Vot U683) by ORICC Research Fund, University Tun Hussein Onn Malaysia (UTHM), Batu Pahat, Johor, Malaysia.

REFERENCES

- [1] A. Boglietti, A. Cavagnino, L. Feraris, and M. Lazzari, "Energy-efficient motors," *IEEE Ind. Electron. Mag.*, vol. 2, no. 4, pp. 32–37, 2008.
- [2] B. C. Mecrow and A. G. Jack, "Efficiency trends in electric machines and drives," *Energy Policy*, vol. 36, no. 12, pp. 4336–4341, Dec. 2008.
- [3] S. E. Rauch and L. J. Johnson, "Design Principles of Flux-Switch Alternators," *Trans. Am. Inst. Electr. Eng. Part III Power Appar. Syst.*, vol. 74, no. 3, pp. 1261–1268, 1955.
- [4] R. L. Owen, Z. Q. Zhu, and G. W. Jewell, "Hybrid Excited Flux-Switching Permanent Magnet Machines," in *Power Electronics and Applications, 2009. EPE '09. 13th European Conference on*, 2009, vol. 46, no. 6, pp. 1726–1729.
- [5] C. Liu, J. Zhu, Y. Wang, G. Lei, Y. Guo, and X. Liu, "A Low-Cost Permanent Magnet Synchronous Motor with SMC and Ferrite PM," in *Electrical Machines and Systems (ICEMS), 2014 17th International Conference on*, 2014, pp. 397–400.
- [6] E. Spooner, "Hybrid excitation of AC and DC machines," *Fourth Int. Conf. Electr. Mach. Drives*, pp. 48–52, 1989.
- [7] C. Zhao and Y. Yan, "A review of development of hybrid excitation synchronous machine," in *Proceedings of the IEEE International Symposium on Industrial Electronics, 2005. ISIE 2005.*, 2005, vol. 2, pp. 857–862 vol. 2.
- [8] J. T. Chen, Z. Q. Zhu, S. Iwasaki, and R. P. Deodhar, "Influence of Slot Opening on Optimal Stator and Rotor Pole Combination and Electromagnetic Performance of Switched-Flux PM Brushless AC Machines," *IEEE Transactions on Industry Applications*, vol. 47, no. 4, pp. 1681–1691, 2011.
- [9] M. F. Omar, M. Z. Ahmad, E. Sulaiman, H. Soomro, and J. Abd Rani, "Preliminary Study of a New Topology of Permanent Magnet Flux Switching Motor for Electric Buses," in *2017 International Conference on Electrical, Electronic, Communication and Control Engineering (ICEECC2017)*, 2017.
- [10] J. H. Hu, L. Wang, J. B. Zou, and B. Zhao, "Cogging torque reduction of hybrid excitation flux switching motor," *Proc. - 5th Int. Conf. Instrum. Meas. Comput. Commun. Control. IMCCC 2015*, vol. 2, no. 5, pp. 1889–1892, 2016.